Computational Comparison of S_N2 Substitution Reactions of $CHX^{\bullet-}$ and CH_2X^- with CH_3X (X = Cl, Br). Do Open-Shell and Closed-Shell Anions React Differently?

Michael L. McKee

Department of Chemistry, Auburn University, Auburn, Alabama 36849

Received January 29, 1997 (Revised Manuscript Received September 15, 1997[⊗]*)*

The S_N2 displacement reaction of the radical anions ($CHCl^{\bullet-}$ and $CHBr^{\bullet-}$) and the closed-shell anions (CH_2Cl^- and CH_2Br^-) with CH_3Cl and CH_3Br were studied with density functional theory. It was determined that the anions CH_2Cl^- and CH_2Br^- were more reactive than the radical anions $CHCl^{\bullet-}$ and $CHBr^{\bullet-}$, in agreement with experiment. The degree of charge transfer in the reactant complex is the best indicator of the reactivity trend. It was found that two reactions (CH_2Cl^- with CH_3Cl and CH_3Br) proceeded without an activation barrier at the B3LYP/6-31+G(d) level. The backside transition states (leading to inversion of configuration at the methyl group) were 20−30 kcal/mol lower in energy than the frontside transition states (leading to retention of configuration). Interestingly, it was found that the mechanism of backside and frontside attack by radical anions was different. In backside attack, the radical anion leads with the lone pair directed toward the methyl group to form an incipient two-center, two-electron bond. In frontside attack, the radical anion leads with the unpaired electron directed toward the methyl group to form an incipient two-center, one-electron bond.

Introduction

Bimolecular substitution (S_N2) reactions have received close scrutiny both in the gas and solution phase.[1−7] In the gas phase,[1] a central barrier exists flanked by reactant and product complexes. In solution,[1] the central barrier is often found to be higher (less solvation of the transition state due to delocalization of charge) and the two complexes often disappear. Much work has been devoted to the study of factors which influence reactivity. For example, the activation barriers of reactions involving anions as nucleophiles of the type $X^- + CH_3X \rightarrow XCH_3 + X^-$ have been found to correlate with the methyl cation affinity (MCA) of the reactant ion.[8] However, recent theoretical results[9] suggest that, while the methyl cation affinities of X^- (X = Cl, Br, I) correlate with the central barrier, the MCA of F^- does not.

Pross and Shaik[4,10] have developed a qualitative means of predicting relative barrier heights using a state correlation diagram (SCD). This method relates the difference in energy between two configurations in the reactant complex to the overall barrier. A large energy separation between configurations would imply a large activation barrier. They used this approach to rationalize the observation[11] that radical cations were sometimes found to be rather resistant to nucleophilic attack. For reactions of closed-shell cations, the configurations differed by one electron, while for reactions involving a radical cation, the configurations differed by two electrons. An alternative point of view would be that radical cations require additional activation (relative to the closed-shell cations) corresponding to promotion of an electron before reaction of the nucleophile can occur.

A recent experimental study by Nibbering and coworkers[12,13] considered reactions of $CHX^{\bullet-}$ and CH_2X^- with CH_3X (X = Cl,Br) in a Fourier transform ion cyclotron resonance instrument to determine whether radical anions ($CHX^{\bullet-}$) reacted differently from anions (CH_2X^-). They postulated that the mechanism was S_N2 (eq 1) because the alternative mechanism (eq 2), a single-

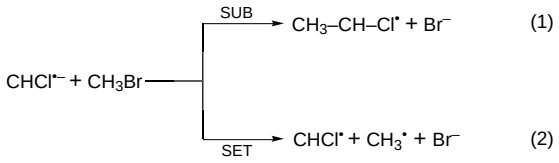

electron-transfer reaction of the radical anion with CH_3X, was excluded by thermodynamic considerations.[12]

They concluded that the S_N2 substitution reactions of the carbene radical anions ($CHCl^{\bullet-}$ or $CHBr^{\bullet-}$) are less efficient than those of substituted methyl anions (CH_2Cl^-

[⊗] Abstract published in *Advance ACS Abstracts,* November 1, 1997.

(1) Harris, J. M.; McManus, S. P., Eds.; *Nucleophilicity*; Advances in Chemistry Series 215; American Chemical Society: Washington DC, 1987.
(2) Vetter, R.; Zülicke, L. *J. Am. Chem. Soc.* **1990**, *112*, 5137.
(3) (a) Shi, Z.; Boyd, R. J. *J. Am. Chem. Soc.* **1990**, *112*, 6789. (b) Boyd, R. J.; Kim. C.-K.; Shi, Z.; Weinberg, N.; Wolfe, S. *J. Am. Chem. Soc.* **1993**, *115*, 10147.
(4) Shaik, S. S.; Schlegel, H. B.; Wolfe, S. *Theoretical Aspects of Physical Organic Chemistry, The S_N2 Mechanism*; Wiley: New York, 1992.
(5) Minkin, V. I.; Simkin, B. Y.; Minyaev, R. M. *Quantum Chemistry of Organic Copounds--Mechanisms of Reactions*; Springer-Verlag: Berlin, 1990.
(6) Riveros, J. M.; José, S. M.; Takashima, K. *Adv. Phys. Org. Chem.* **1985**, *21*, 197.
(7) Marcus, R. A. *J. Phys. Chem. A* **1997**, *101*, 4072.
(8) Pellerite, M. J.; Brauman, J. I. *J. Am. Chem. Soc.* **1983**, *105*, 2672.
(9) Glukhovtsev, M. N.; Pross, A.; Radom, L. *J. Am. Chem. Soc.* **1995**, *117*, 2024.
(10) (a) Shaik, S. S.; Pross, A. *J. Am. Chem. Soc.* **1989**, *111*, 4306. (b) Eberson, L.; Shaik, S. *J. Am. Chem. Soc.* **1990**, *112*, 4484.
(11) (a) Eberson, L. *Electron-Transfer Reactions in Organic Chemistry*; Springer-Verlag: Heidelberg, 1987. (b) Zipse, H. *J. Am. Chem. Soc.* **1995**, *117*, 11798.
(12) Born, M.; Ingemann, S.; Nibbering, N. M. M. *J. Chem. Soc., Perkin Trans. 2* **1996**, 2537.
(13) Born, M.; Ingemann, S.; Nibbering, N. M. M. *J. Am. Chem. Soc.* **1994**, *116*, 7210.

S0022-3263(97)00163-1 CCC: $14.00 © 1997 American Chemical Society

Table 1. Total Energies (hartrees) and Thermodynamic Properties (kcal/mol) of Various Reactant and Product Species Optimized at the B3LYP/6-31+G(d) Level

	PG	ES	B3LYP/6-31+G(d)	B3LYP/6-311+G(2d,p)	ZPE (NIF)[a]	C_p, 298 K[b]	S, 298 K[c]
CH_3^+	D_{3h}	$^1A_1'$	−39.480 39	−39.492 12	19.82 (0)	2.38	44.61
CH_3	D_{3h}	$^2A_2''$	−39.842 64	−39.856 10	18.77 (0)	2.51	46.54
Cl^-	K_h	^1S	−460.274 72	−460.303 73	0.00 (0)	1.78	36.65[d]
CHCl	C_s	$^1A'$	−498.765 97	−498.809 28	7.07 (0)	2.43	56.17
CHCl	C_s	$^3A''$	−498.761 40	−498.802 78	7.22 (0)	2.43	57.86
$CH_2Cl^\bullet$	C_s	$^2A'$	−499.442 51	−499.484 88	14.26 (0)	2.84	61.12
$CHCl^{\bullet-}$	C_s	$^2A''$	−498.818 77	−498.861 08	6.08 (0)	2.57	58.85
CH_2Cl^-	C_s	$^1A'$	−499.466 37	−499.511 82	13.84 (0)	2.61	58.61
CH_3Cl	C_{3v}	$^1A_1$	−500.111 52	−500.154 54	23.86 (0)	2.49	55.99
CH_3CH_2Cl	C_s	$^1A'$	−539.430 45	−539.483 89	42.01 (0)	3.12	65.68
$CH_3CHCl^\bullet$	C_s	$^2A''$	−538.766 01	−538.818 71	32.28 (1)	3.10	66.92
$CH_3CHCl^\bullet$	C_1	^2A	−538.766 15	−538.818 82	32.70 (0)	3.38	68.52
Br^-	K_h	^1S	−2571.803 18	−2574.232 87	0.00 (0)	1.78	39.08[d]
CHBr	C_s	$^1A'$	−2610.287 18	−2612.723 28	6.80 (0)	2.75	58.94
CHBr	C_s	$^3A''$	−2610.282 30	−2612.717 15	6.92 (0)	2.46	60.58
$CH_2Br^\bullet$	C_s	$^2A'$	−2610.962 13	−2613.398 91	13.83 (0)	2.95	64.84
$CHBr^{\bullet-}$	C_s	$^2A''$	−2610.346 98	−2612.784 00	5.98 (0)	2.59	61.50
CH_2Br^-	C_s	$^1A'$	−2610.994 69	−2613.435 17	13.68 (0)	2.63	61.24
CH_3Br	C_{3v}	$^1A_1$	−2611.632 43	−2614.070 44	23.50 (0)	2.53	58.75
CH_3CH_2Br	C_s	$^1A'$	−2650.952 93	−2653.399 20	41.67 (0)	3.19	68.41
$CH_3CHBr^\bullet$	C_s	$^2A''$	−2650.287 34	−2652.732 30	31.95 (1)	3.18	69.67
$CH_3CHBr^\bullet$	C_1	^2A	−2650.287 54	−2652.732 52	32.37 (0)	3.44	71.21

[a] Zero-point energies in kcal/mol with the number of imaginary frequencies in parentheses. [b] Heat capacities integrated to 298 K in kcal/mol. [c] Entropies in cal/mol K. [d] Chase, M. W., Jr.; Davies, C. A.; Downey, J. R., Jr.; Frurip, D. J.; McDonald, R. A.; Syverud, A. N. *J. Phys. Chem. Ref. Data* **1985**, *14*, Suppl. 1.

or CH_2Br^-) with CH_3Cl and CH_3Br. Furthermore, they attributed the reactivity difference to a difference in ionization energies of the nucleophile. However, conclusions about the precise nature of the reaction were tentative because "the transition state involved in the crucial steps of these gas-phase reactions is still unknown, in particular with respect to the electronic coupling between the various reactant (radical) anions and the selected substrates." [12] The present work was undertaken to compare the nature of S_N2 substitution reactions of radical anions ($CHCl^{\bullet-}$ and $CHBr^{\bullet-}$) and closed-shell anions (CH_2Cl^- and CH_2Br^-) with CH_3Cl and CH_3Br.

Method

All calculations were made with the Gaussian program system.[14] Geometries were optimized using the B3LYP exchange/correlation functional combination, which has proven to be extremely effective in describing a number of molecular properties.[15] The 6-31+G(d) basis set was used for geometry optimization, while single-point calculations were made with the 6-311+G(2d,p) basis set.[14] The calculated frequencies were used to compute entropies and a heat capacity correction to 298 K.

Six reactions were studied (eq 3−8) which are described by

$$CH_2Cl^- + CH_3Cl \longrightarrow CH_3CH_2Cl + Cl^- \text{ (reaction } \mathbf{1}\text{)} \quad (3)$$

$$CHCl^{\bullet-} + CH_3Cl \longrightarrow CH_3CHCl^\bullet + Cl^- \text{ (reaction } \mathbf{2}\text{)} \quad (4)$$

$$CH_2Cl^- + CH_3Br \longrightarrow CH_3CH_2Cl + Br^- \text{ (reaction } \mathbf{3}\text{)} \quad (5)$$

$$CHCl^{\bullet-} + CH_3Br \longrightarrow CH_3CHCl^\bullet + Br^- \text{ (reaction } \mathbf{4}\text{)} \quad (6)$$

$$CH_2Br^- + CH_3Cl \longrightarrow CH_3CH_2Br + Cl^- \text{ (reaction } \mathbf{5}\text{)} \quad (7)$$

$$CHBr^{\bullet-} + CH_3Cl \longrightarrow CH_3CHBr^\bullet + Cl^- \text{ (reaction } \mathbf{6}\text{)} \quad (8)$$

giving the designation of **1**−**6** followed by a label to indicate the position along the reaction path. Using eq 4 as an example, the reaction proceeds from reactants $CHCl^{\bullet-}/CH_3Cl$ (**2-r**) through an ion−molecule complex (**2-c**), a backside S_N2 (**2-tsb**), or frontside (**2-tsf**) transition state to products $CH_3CHCl^\bullet/Cl^-$ (**2-p**). A product complex will also exist but has not been calculated.

Total energies (hartrees), zero-point energies (kcal/mol), heat capacities integrated to 298 K (kcal/mol), and entropies (cal/mol K) are given in Table 1 for reactant species and in Table 2 for species along the reaction profile for reactions **1**−**6**. Molecular drawings of relevant species are given in Figure 1. Table 3 presents relative energies, enthalpies (298 K), and free energies (298 K) along the reaction profiles. Unless otherwise noted, the discussion below will refer to enthalpies at 298 K computed at the B3LYP/6-311+G(2d,p)//B3LYP/6-31+G(d) level.

Ab initio theory was used to check the results of density functional theory for reactions **1**−**6**. Geometries were optimized at the MP2/6-31+G(d) level, and single-point calculations were made at the QCISD(T)/6-31+G(d) and MP2/6-311+G(2d,p) levels and combined[16] to estimate the full [QCISD(T)/6-311+G(2d,p)] energy. Zero-point corrections (scaled by 0.95) were made with MP2/6-31+G(d) frequencies. Binding energies of the ion−molecule complex are greater by an average of 0.9 kcal/mol, while activation barriers are an average of 2.5 kcal/mol larger than at DFT (Table 3).

(14) Frisch, M. J.; Trucks, G. W.; Schlegel, H. B.; Gill, P. M. W.; Johnson, B. G.; Robb, M. A.; Cheeseman, J. R.; Keith, T.; Petersson, G. A.; Montgomery, J. A.; Raghavachari, K.; Al-Laham, M. A.; Zakrzewski, V. G.; Ortiz, J. V.; Foresman, J. B.; Cioslowski, J.; Stefanov, B. B.; Nanayakkara, A.; Challacombe, M.; Peng, C. Y.; Ayala, P. Y.; Chen, W.; Wong, M. W.; Andres, J. L.; Replogle, E. S.; Gomperts, R.; Martin, R. L.; Fox, D. J.; Binkley, J. S.; Defrees, D. J.; Baker, J.; Stewart, J. P.; Head-Gordon, M.; Gonzalez, C.; Pople, J. A. *Gaussian94* (Rev. B.1), Gaussian, Inc.; Pittsburgh PA, 1995.

(15) (a) Bartolotti, L. J.; Flurchick, K. An Introduction to Density Functional Theory. In *Reviews in Computational Chemistry*; Lipkowitz, K. B., Boyd, D. B., Eds.; VCH: New York, 1996; Vol 7. (b) Parr, R. G.; Yang, W. *Density-Functional Theory of Atoms and Molecules*; Oxford Press: Oxford, 1989. (c) Ziegler, T. *Chem. Rev. (Washington, D.C.)* **1991**, *91*, 651. (d) *Density Functional Methods in Chemistry*; Labanowski, J. K., Andzelm, J. W., Eds.; Springer: Berlin, 1991. (e) Johnson, B. G.; Gill, P. M. W.; Pople, J. A. *J. Chem. Phys.* **1993**, *98*, 5612. (f) Gill, P. M. W.; Johnson, B. G.; Pople, J. A.; Frisch, M. J. *Chem. Phys. Lett.* **1992**, *197*, 499. (g) Raghavachari, K.; Strout, D. L.; Odom, G. K.; Scuseria, G. E.; Pople, J. A.; Johnson, B. G.; Gill, P. M. W. *Chem. Phys. Lett.* **1993**, *214*, 357. (h) Raghavachari, K.; Zhang, B.; Pople, J. A.; Johnson, B. G.; Gill, P. M. W. *Chem. Phys. Lett.* **1994**, *220*, 1994. (i) Johnson, B. G.; Gonzales, C. A.; Gill, P. M. W.; Pople, J. A. *Chem. Phys. Lett.* **1994**, *221*, 100. (j) Baker, J.; Scheiner, A.; Andzelm, J. *Chem. Phys. Lett.* **1993**, *216*, 380. (k) Becke, A. D. *J. Chem. Phys.* **1993**, *98*, 5648.

(16) Additivity approximation: $\Delta E[\text{QCISD(T)/6-311+G(2d,p)}] = \Delta E(\text{QCISD(T)/6-31+G(d)}) + \Delta E(\text{MP2/6-311+G(2d,p)}) - \Delta E(\text{MP2/6-31+G(d)})$.

Table 2. Total Energies (hartrees) and Thermodynamic Properties (kcal/mol) of Various Complexes and Transition States Calculated at the B3LYP/6-31+G(d) Level

	PG	ES	B3LYP/6-31+G(d)	B3LYP/6-311+G(2d,p)	ZPE (NIF)[a]	C_p, 298 K	S, 298 K
1-r			−999.577 89	−999.666 36	37.70 (0)	5.10	114.60
1-tsf	C_s	^{1}A′	−999.551 48	−999.639 78	37.81 (1)	4.93	84.13
1-p			−999.705 17	−999.787 62	42.01 (0)	4.90	102.33
2-r			−998.930 29	−999.015 62	29.94 (0)	5.06	114.84
2-c	C_s	^{2}A″	−998.947 42	−999.032 61	30.56 (0)	5.56	93.77
2-tsb	C_s	^{2}A″	−998.945 07	−999.030 26	30.21 (1)	5.17	90.93
2-tsf	C_1	^{2}A	−998.899 02	−998.985 54	29.46 (1)	5.07	87.69
2-p			−999.040 87	−999.122 55	32.70 (0)	5.16	105.17
3-r			−3111.098 80	−3113.582 26	37.34 (0)	5.14	117.36
3-tsf	C_s	^{2}A′	−3111.080 40	−3113.563 75	37.63 (1)	5.00	86.80
3-p			−3111.233 63	−3113.716 76	42.01 (0)	4.90	104.76
4-r			−3110.451 20	−3112.931 52	29.58 (0)	5.10	117.60
4-c	C_s	^{2}A″	−3110.474 50	−3112.950 50	30.22 (0)	5.59	96.38
4-tsb	C_1	^{2}A	−3110.474 44[a]	−3112.950 58	30.02 (1)	5.18	93.81
4-tsf	C_1	^{2}A	−3110.429 09	−3112.911 45	29.02 (1)	5.24	91.20
4-p			−3110.569 33	−3113.051 69	32.70 (0)	4.90	104.76
5-r			−3111.106 21	−3113.589 71	37.54 (0)	5.12	117.23
5-c	C_s	^{1}A′	−3111.126 05	−3113.606 86	38.18 (0)	5.54	92.52
5-tsb	C_s	^{1}A′	−3111.125 93	−3113.606 66	38.03 (1)	5.04	88.17
5-tsf	C_s	^{1}A′	−3111.079 75	−3113.558 40	37.71 (1)	4.96	86.71
5-p			−3111.227 65	−3113.702 93	41.67 (0)	4.97	105.06
6-r			−3110.458 50	−3112.938 54	29.84 (0)	5.08	117.49
6-c	C_s	^{2}A″	−3110.476 10	−3112.954 00	30.54 (0)	5.54	94.72
6-tsb	C_1	^{2}A	−3110.472 32[b]	−3112.949 81	30.04 (1)	5.25	94.92
6-tsf	C_1	^{2}A	−3110.425 88	−3112.904 12	29.69 (1)	4.95	88.48
6-p			−3110.562 26	−3113.036 25	32.37 (0)	5.22	107.86

[a] A stationary point with two imaginary frequencies was 0.00002 hartrees higher in energy. [b] A stationary point with two imaginary frequencies was 0.00008 hartrees higher in energy.

The two methods show the largest deviation for the frontside activation barriers (**2-tsf**, 5.3 kcal/mol; **4-tsf**, 6.3 kcal/mol; and **6-tsf**, 4.4 kcal/mol). MP2/6-31+G(d) geometries (not shown) are very similar to B3LYP/6-31+G(d) geometries, except in the case of **4-tsf**, where spin contamination was a serious problem ($\langle S^2 \rangle = 1.34$). It should be noted that the forming C−C bond in the backside and frontside transition states are about 0.1−0.2 Å shorter by ab initio compared to DFT theory.

In contrast to the DFT results, an ion−molecule complex and backside transition state were located at the MP2/6-31+G(d) level for reaction 1 (**1-c** and **1-tsb**). The activation barrier for backside attack in reaction 1 at the [QCISD(T)/6-311+G(2d,p)]+ZPC level (1.0 kcal/mol) is lower than the corresponding values for backside attack in reactions **2** and **4**−**6**. Since a small activation barrier is consistent with experimental results,[12] it is probable that the DFT method used here underestimates activation barriers by a small amount, a known tendency.[17]

As part of a recent study on proton-transfer reactions, Van Verth et al.[18] calculated the ion−molecule complex (**1-c**) and backside transition state (**1-tsb**). Their activation energy at the MP4/6-31+G(d)//HF/6-31+G(d) level (1.2 kcal/mol) is very close to the barrier calculated in this work at the [QCISD(T)/6-311+G(2d,p)]//MP2/6-31+G(d)+ZPC level (1.0 kcal/mol).

While CH_2Cl^- and CH_3Br collapsed to products (CH_3CH_2Cl plus Br^-) with the DFT method without forming a complex, at the MP2/6-31+G(d) level an ion−molecule complex (**3-c**) was located with the standard optimization procedure and normal stopping criterion. However, the complex was characterized by a very small vibrational mode (6 cm^{-1}), and when the complex was reoptimized using the analytical Hessian matrix, the optimization proceeded to products (CH_3CH_2Cl plus Br^-). Thus, it appears that reaction 3 does not have a well-characterized minimum corresponding to an ion−molecule complex.

To summarize, barriers by DFT are about 2.5 kcal/mol higher than by conventional ab initio theory. While the ion−molecule complexes **1-c** and **3-c** do not exist at DFT, a well-defined ion−molecule complex does exist for **1-c** at MP2/6-31+G(d) but not for **3c**. The trends in activation barriers are very similar between the two methods. Since the trends appear to be more regular with DFT and given the fact that spin contamination is not a problem, the DFT results will be used to interpret reactivity.

Results and Discussion

Before discussing the S_N2 reactions, a comparison will be made between experiment and theory for the reactant and product fragments in order to determine the accuracy of the computational method. Relevant ionization energies (IE), proton affinities (PA), bond dissociation enthalpies (BDE), methyl cation affinities (MCA), and singlet−triplet splittings (S−T) are collected in Table 4 and compared with available experimental data.[19] The average deviations are 3 kcal/mol for ionization energies, 2 kcal/mol for proton affinities, and 3 kcal/mol for bond dissociation enthalpies. The B3LYP/6-31+G(d) method overestimates the C−Cl bond in CH_3Cl by 0.030 Å (1.806 Å, calcd; 1.776 Å, exptl[20]) and the C−Br bond in CH_3Br by 0.031 Å (1.965 Å, calcd; 1.934 Å, exptl[21]). The optimized geometries of $CH_3CHCl^\bullet$ and $CH_3CHBr^\bullet$ both had one imaginary frequency for the C_s-symmetry species. Reoptimizing in C_1 symmetry lowered the energies by only 0.1 kcal/mol and produced no imaginary frequencies. Including zero-point corrections reversed the relative stabilities in favor of the symmetrical structures. However, using the C_s-symmetry structure as reference presents a dilemma[22] since a very low-frequency mode, which would make a large contribution to the heat

(17) (a) Lim, M. H.; Worthington, S. E.; Dulles, F. J.; Cramer, C. J. In *Density Functional Methods in Chemistry*; ASC Symposium Series 629; Laird, B. B., Ross, R. B., Ziegler, T., Eds.; American Chemical Society: Washington, DC, p 402. (b) Worthington, S. E.; Cramer, C. J. *J. Phys. Org. Chem.* In press.

(18) Van Verth, J. E.; Saunders, W. H., Jr. *J. Org. Chem.* **1997**, *62*, 5743.

(19) Lias, S. G.; Bartmess, J. E.; Liebman, J. F.; Holmes, J. L.; Levin, R. D.; Mallard, W. G. *J. Phys. Chem. Ref. Data* **1988**, *17*, Suppl. No. 1.

(20) Jensen, T.; Brodersen, S.; Guelachvili, G. *J. Mol. Spectrosc.* **1981**, *88*, 378.

(21) Graner, G. *J. Mol. Spectrosc.* **1981**, *90*, 394.

(22) For a discussion of this dilemma see: Müller, H.; Kutzelnigg, W.; Noga, J.; Klopper, W. *J. Chem. Phys.* **1997**, *106*, 1863.

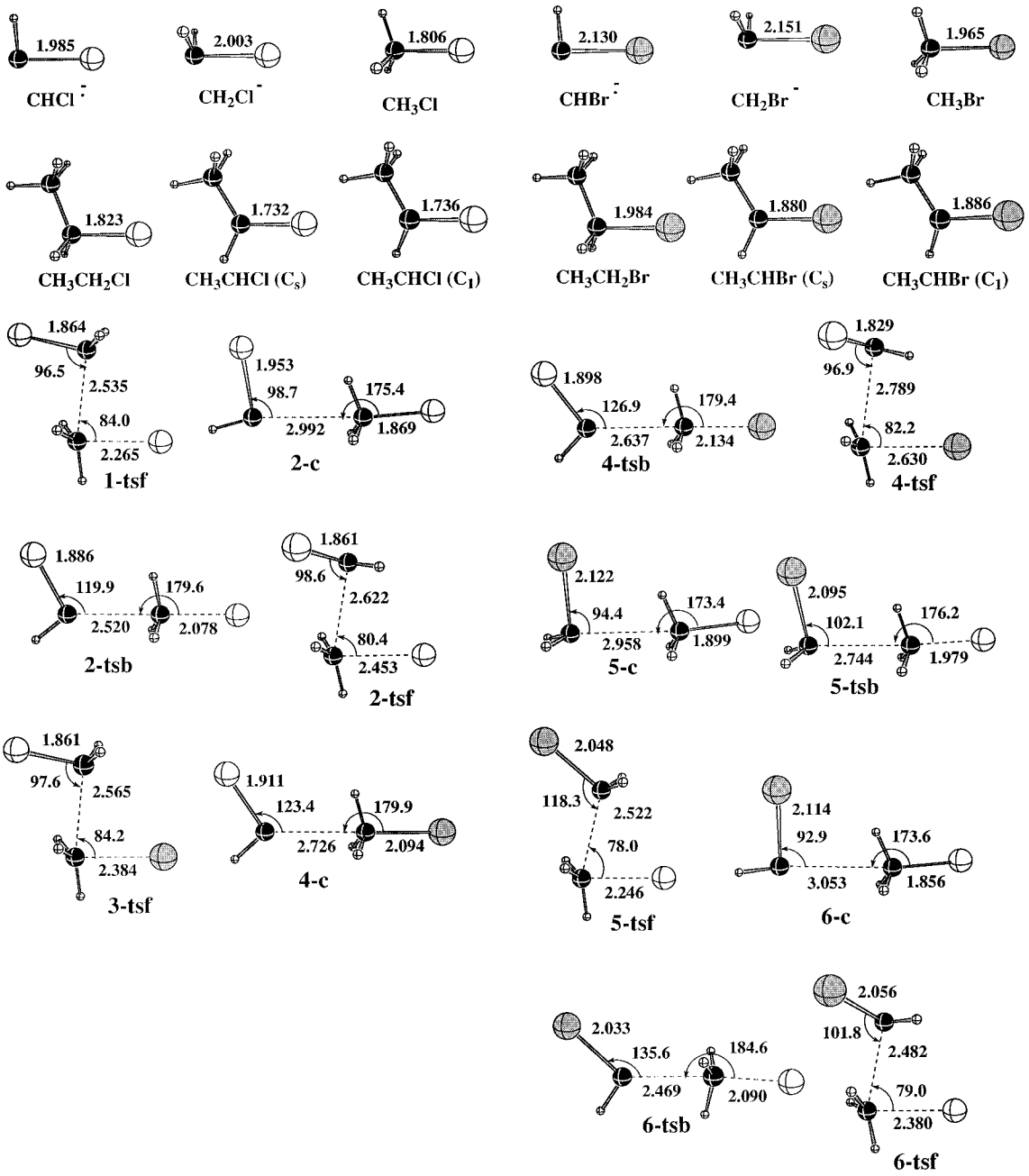

Figure 1. Selected geometric parameters of various species optimized at the B3LYP/6-31+G(d) level.

capacity and entropy, is not included because it is imaginary. For that reason, the C_1-symmetry structures will be used as a references for $CH_3CHCl^{\bullet}$ and $CH_3CHBr^{\bullet}$. For both radicals ($CH_3CHCl^{\bullet}$ and $CH_3CHBr^{\bullet}$), the distortion is caused by a preferred pyramidalization around the −CHX group.

The orientation in a ion−molecule complex involving X^- and CH_3X has been determined from theory[9] to be a symmetric interaction of X^- with the three hydrogens of CH_3X ($X\cdots H_3CX^-$). The ion−molecule complexes formed between $CHCl^{\bullet -}/CH_3Cl$ (**2-c**), $CHCl^{\bullet -}/CH_3Br$ (**4-c**), CH_2Br^-/CH_3Cl (**5-c**), and $CHBr^{\bullet -}/CH_3Cl$ (**6-c**) all have similar interactions; i.e., the negatively charged carbon is directed toward all three of the methyl halide hydrogens (Figure 1). For the pairs CH_2Cl^-/CH_3Cl and CH_2Cl^-/CH_3Br (reactions 1 and 3), a complex could not be located because the S_N2 displacement of a halide ion from CH_3X occurred without an activation barrier. The binding enthalpies for the complexes (**2-c**, **4-c**, **5-c**, and **6-c**) varied from a low of 8.5 kcal/mol to a high of 10.8 kcal/mol (9.6, 10.8, 9.8, and 8.5 kcal/mol, respectively). For comparison, a binding enthalpy (298 K) of 10.4 kcal/mol has been calculated[9] for $Cl\cdots H_3CCl^-$ at the G2(+) level of theory.

The ion−molecule interactions in the complex are not only electrostatic, but also include charge transfer from the nucleophile to the methyl halide. Computed charges using the NPA (natural population analysis) method[23] indicate that from 0.04 (**6-c**) to 0.15 (**4-c**) electron is transferred from the nucleophile to the methyl halide in the complex (Table 5). Since the degree of charge transfer is a function of the donor ability of the nucleophile and acceptor ability of the electrophile, it provides

(23) (a) Forster, J. P.; Weinhold, *J. Am. Chem. Soc.* **1980**, *102*, 7211. (b) Reed, A. E.; Weinhold, F. *J. Chem. Phys.* **1983**, *78*, 4066. (c) Reed, A. E.; Weinstock, R. B.; Weinhold, F. *J. Chem. Phys.* **1985**, *83*, 735. (d) Carpenter, J. E.; Weinhold, F. *J. Mol. Struct. (THEOCHEM)* **1988**, *41*, 169. (e) Reed, A. E.; Curtiss, L. A.; Weinhold, F. *Chem. Rev. (Washington, D.C.)* **1988**, *88*, 899.

Table 3. Relative Energies (kcal/mol) and Thermodynamic Values for Reactions 1−6 Optimized at the B3LYP/6-31+G(d) Level

	B3LYP/ 6-31+G(d)	B3LYP/ 6-311+G(2d,p)	+ZPC	Δ*H*, 298 K	Δ*G*, 298 K	[QCISD(T)/ 6-311+G (2d,p)] +ZPC[a]
1-r	0.0	0.0	0.0	0.0	0.0	0.0
1-c						−11.9
1-tsb						−10.9
1-tsf	16.6	16.7	16.8	16.6	25.7	18.2
1-p	−79.9	−76.1	−71.8	−72.0	−68.4	
2-r	0.0	0.0	0.0	0.0	0.0	0.0
2-c	−10.7	−10.7	−10.1	−9.6	−3.3	−11.2
2-tsb	−9.3	−9.2	−8.9	−8.8	−1.7	−7.2
2-tsf	19.6	18.9	18.4	18.4	26.5	23.7
2-p	−69.4	−67.1	−64.3	−62.2	−59.3	
3-r	0.0	0.0	0.0	0.0	0.0	0.0
3-c						−12.8[b]
3-tsf	11.5	11.6	11.9	11.8	20.9	13.2
3-p	−84.6	−84.4	−79.7	−79.9	−72.4	
4-r	0.0	0.0	0.0	0.0	0.0	0.0
4-c	−14.6	−11.9	−11.3	−10.8	−4.5	−11.5
4-tsb	−14.6	−12.0	−11.6	−11.5	−4.4	−9.5
4-tsf	13.9	12.6	12.0	12.1	20.0	18.3[c]
4-p	−74.1	−75.4	−72.3	−72.5	−68.7	
5-r	0.0	0.0	0.0	0.0	0.0	0.0
5-c	−12.4	−10.8	−10.2	−9.8	−2.4	−11.0
5-tsb	−12.4	−10.6	−10.1	−10.2	−1.5	−9.5
5-tsf	16.6	19.6	19.8	19.6	28.7	20.4
5-p	−76.2	−71.0	−66.9	−67.1	−63.5	
6-r	0.0	0.0	0.0	0.0	0.0	0.0
6-c	−11.0	−9.7	−9.0	−8.5	−1.7	−10.5
6-tsb	−8.7	−7.1	−7.0	−7.1	0.9	−5.5
6-tsf	20.5	21.6	21.4	24.3	32.9	25.8
6-p	−65.1	−61.3	−58.8	−58.7	−55.8	

[a] Geometries optimized at the MP2/6-31+G(d) level. Single point energies calclated at the QCISD(T)/6-31+G(d) and MP2/6-311+G(2d,p) levels and combined. Zero-point (0.95 scaling factor) corrections were made using MP2/6-31+G(d) frequencies. [b] The lowest vibrational frequency of the initially optimized complex was 6 cm^{-1}. When the geometry was reoptimized starting with the anaytically calculated Hessian, the complex disappeared and only products ($CH_3CH_2Cl + Br^-$) were obtained. [c] The MP2/6-31+G(d) energy suffers from considerable spin contamination ($\langle S^2 \rangle = 1.34$).

Table 4. Comparison of Calculated and Experimental Proton Affinities (PA), Bond Dissociation Enthalpies (BDE), Ionization Energies (IE), Methyl Cation Affinities (MCA), and Singlet-Triplet Splitting (S−T) (kcal/mol)[a]

	Δ*H* (298 K)	
	calcd	exptl[b]
(PA) $CH_2Cl^\bullet \rightarrow CHCl^{\bullet -} + H^+$	384.7	384.8
(PA) $CH_2Br^\bullet \rightarrow CHBr^{\bullet -} + H^+$	379.4	380.7
(PA) $CH_3Cl \rightarrow CH_2Cl^- + H^+$	395.2	396.0
(PA) $CH_3Br \rightarrow CH_2Br^- + H^+$	390.7	396.7
(BDE) $CH_2Cl^{\bullet -} \rightarrow CHCl^{\bullet -} + H$	70.2	
(BDE) $CH_2Br^{\bullet -} \rightarrow CHBr^{\bullet -} + H$	64.8	
(BDE) $CH_3Cl \rightarrow CH_2Cl^\bullet + H$	97.6	100.9 (99.4)[c]
(BDE) $CH_3Br \rightarrow CH_2Br^\bullet + H$	98.8	102.0 (100.8)[c]
(BDE) $CH_3CH_2Cl \rightarrow CH_3CHCl^\bullet + H$	94.9	
(BDE) $CH_3CH_2Br \rightarrow CH_3CHBr^\bullet + H$	95.9	
(IE) $CHCl^{\bullet -} \rightarrow CHCl + e^-$	33.2	28.0 (30.2)[d]
(IE) $CH_2Cl^- \rightarrow CH_2Cl^\bullet + e^-$	17.5	18.4
(IE) $CHBr^{\bullet -} \rightarrow CHBr + e^-$	39.2	33.5
(IE) $CH_2Br^- \rightarrow CH_2Br^\bullet + e^-$	22.8	22.9
(MCA) $CH_3CHCl^\bullet \rightarrow CH_3^+ + CHCl^{\bullet -}$	287.3	
(MCA) $CH_3CH_2Cl \rightarrow CH_3^+ + CH_2Cl^-$	294.7	
(MCA) $CH_3CHBr^\bullet \rightarrow CH_3^+ + CHBr^{\bullet -}$	281.3	
(MCA) $CH_3CH_2Br \rightarrow CH_3^+ + CH_2Br^-$	289.7	
(BDE) $CH_3CHCl^\bullet \rightarrow CH_3 + CHCl$	91.6	
(BDE) $CH_3CH_2Cl \rightarrow CH_3 + CH_2Cl$	82.9	
(BDE) $CH_3CHBr^\bullet \rightarrow CH_3 + CHBr$	91.7	
(BDE) $CH_3CH_2Br \rightarrow CH_3 + CH_2Br$	83.7	
(S−T) CHCl ($^1A' \rightarrow {}^3A''$)	4.3	6.4[e] (4.2)[f]
(S−T) CHBr ($^1A' \rightarrow {}^3A''$)	3.6	

[a] The energies of H at the B3LYP/6-31+G(d) and B3LYP/6-311+G(2d,p) levels are −0.50027 and −0.50216 hartrees, respectively. [b] See ref 12. [c] Holmes, J. L.; Lossing, F. P. *J. Am. Chem. Soc.* **1988**, *110*, 7343. [d] Based on a more recent determination of the heat of formation of CHCl. See: Poutsma, J. C.; Paulino, J. A.; Squires, R. R. *J. Phys. Chem. A* **1997**, *101*, 5327. [e] See Irikura, K. K.; Goddard, W. A., III; Beauchamps, J. L. *J. Am. Chem. Soc.* **1992**, *114*, 48. [f] Gilles, M. K., Ervin, K. M.; Ho, J., Lineberger, W. C. *J. Phys. Chem.* **1992**, *96*, 1130.

a reasonable measure of the tendency to undergo an S_N2 reaction. In fact, the degree of charge transfer in the complex correlates with the S_N2 activation barrier.

Displacement of a halide ion from methyl halide by a nucleophile can occur by backside or frontside attack of the nucleophile. Backside attack leads to inversion of configuration while frontside attack leads to retention of configuration. It is found experimentally that backside attack (i.e. inversion of configuration) is preferred in most instances.[24] While frontside attack might be envisioned when the backside is severely hindered, one must remember that in solution the mechanism may change to S_N1 (halide completely dissociates before the nucleophile enters). The S_N1 mechanism is less likely to compete with the S_N2 frontside mechanism in the gas phase (at low temperatures) due to the large dissociation energy for heterolytic C−X bond cleavage.

Reactions involving backside attack will be considered first. As mentioned above, backside attack of CH_2Cl^- on CH_3Cl and CH_3Br occurred without a calculated activation barrier at the B3LYP/6-31+G(d) level. This would imply that the reactions are controlled by the collision rate constant. Nibbering and co-workers[12] found that $CH_2Cl^- + CH_3Br$ (reaction **3**) was the fastest reaction considered with a rate constant 40% of the theoretical estimate for a collision-controlled (i.e. barrierless) reaction. They found that the rate constants increased in the order (slowest to fastest) **6** < **5** < **4** < **3** with relative rate constants of 1, 2, 5, and 8 (Table 6). Backside transition states were located for the four reactions **2-tsb**, **4-tsb**, **5-tsb**, and **6-tsb**. At the highest level of theory (B3LYP/6-311+G(2d,p)//B3LYP/6-31+G(d) plus thermal corrections), two of the reactions had negative enthalpies of activation (Table 3; **4-c** → **4-tsb**, $\Delta H^\ddagger = -0.7$ kcal/mol, and **5-c** → **5-tsb**, $\Delta H^\ddagger = -0.4$ kcal/mol). To make a comparison of relative rates, the free energies of activation ($\Delta G^\ddagger$) were computed using theoretical entropies. The calculated order of free energies of activation was **6** > **2** > **5** > **4** (Table 6; 2.6, 1.6, 0.9, and 0.1 kcal/mol, respectively). The computed relative rate constants are 1:3:6:12. Presumably, the rate constants for reactions **1** and **3** (no transition state found) would be greater than for reaction **4**.

Computed trends are given in Table 6. The degree of charge transfer in the complex appears to be the best indicator of relative rate constants. As mentioned above, the degree of charge transfer is a function of the donating ability of the nucleophile and the accepting ability of the electrophile. If one considers only the reactions involving CH_3Cl (**1**, **2**, **5**, **6**), the relative rates correlate with the ionization energies (IE) of the anions as well as the methyl cation affinities (MCA). A smaller ionization energy of the anion would indicate that it is a better nucleophile which should react faster with a given methyl halide. Similarly, for constant methyl halide (reactions **2** and **4**), a greater MCA implies a greater reaction exothermicity.

(24) March, J. Advanced Organic Chemistry, 3rd ed.; Wiley and Sons: New York, 1985.

Table 5. Computed NPA Charges at the B3LYP/6-311+G(2d,p) Level

	reactants (**r**)			complex (**c**)			backside TS (**tsb**)			frontside TS (**tsf**)		
reaction	HCX/H_2CX	CH_3	X	HCX/H_2CX	CH_3	X	HCX/H_2CX	CH_3	X	HCX/H_2CX	CH_3	X
1	−1.00	0.08	−0.08							−0.59	0.09	−0.50
2	−1.00	0.08	−0.08	−0.95	0.20	−0.25	−0.76	0.18	−0.42	−0.48	0.08	−0.60
3	−1.00	0.02	−0.02							−0.59	0.05	−0.46
4	−1.00	0.02	−0.02	−0.85	0.05	−0.20	−0.81	0.11	−0.30	−0.42	0.02	−0.60
6	−1.00	0.08	−0.08	−0.91	0.15	−0.24	−0.77	0.18	−0.41	−0.64	0.11	−0.47
6	−1.00	0.08	−0.08	−0.96	0.15	−0.19	−0.77	0.19	−0.42	−0.56	0.10	−0.54

Table 6. Calculated Trends in Reaction Properties of Reactions 1−6

					constant acceptor[e] (CH_3Cl)		
reaction	rel[a] rate (exptl)	$\Delta G^{\ddagger}$ [b] backsides (298 K)	rel[c] rate (298 K)	CT[d] complex	IE[f] (eV)	MCA[g] $HCX^{\bullet -}/H_2CX^-$	constant donor[h] ($CHCl^{\bullet}$) BDE[i] (H_3C-X)
6	1	2.6	1	0.04	39.2	0.0	
2		1.6	3	0.05	33.2	6.4	83.5
5	2	0.9	6	0.09	22.8	8.4	
4	5	0.1	12	0.15			70.7
1		*j*	>13	*j*	17.5	13.4	
3	8	*j*	>13	*j*			

[a] Experimental relative rate constants from ref 12. [b] Calculate free energies of activation (kcal/mol) from Table 3. [c] Calculated relative rate constants ($A:B = \exp(\Delta G^{\ddagger}_B/\Delta G^{\ddagger}_A)$). [d] The degree of charge transfer (CT) in the complex as calculated from NPA charges (see Table 4). [e] Comparisons are made for reactions **1**, **2**, **4**, and **6**, where the substrate is CH_3Cl. [f] Calculated ionization energies (kcal/mol) from Table 4. [g] Calculated methyl cation affinity (MCA) inkcal/mol relative to $CHBr^{\bullet -}$ from reaction **6** (see Table 4). [h] Comparisons are made for reactions **2** and **4**, where the nucleophile is $CHCl^{\bullet -}$. [i] Experimental bond dissociation enthalpies (kcal/mol) from ref 16. [j] The reaction proceeds without a calculated barrier at the B3LYP/6-31+G(d) level.

Table 7. Computed Reaction Exothermicities, Percentage of C−X Bond Cleavage, and Central Barriers of S_N2 Reactions

reaction	ΔH (wrt reactants)[a]	ΔH (wrt complex)[b]	% $C-X^{\ddagger}$ [c]	$\Delta H^{\ddagger}$
6	−58.7	−50.2	13	1.4
2	−62.2	−52.6	11	0.8
5	−67.1	−57.3	4	−0.4
4	−72.5	−61.7	2	−0.7
1	−72.0			
3	−72.9			

[a] Enthalpy of reaction from reactant to product (**r** → **p**). [b] Enthalpy of reaction from complex to product (**c** → **p**). [c] Percentage C−X bond cleavage (% $C-X = 100\ (d^{\ddagger}_{C-X} - d^{C}_{C-X})/d^{C}_{C-X}$). See ref 25. [d] Activation enthalpy in kcal/mol.

Table 8. Thermodynamic Quantities (kcal/mol) for the Reaction $Y^- + CH_3X$ to $Y + CH_3 + X^-$ (SET) or to $YCH_3 + X^-$ (SUB)

reaction	Y^-	CH_3X	ΔH_{SET}[a]	ΔH_{SUB}[b]	G_{SET}[c]	α[d]	C−C[e]
1	$ClCH_2$	Cl	10.9	−72.0	71.2	0.58	no TS
2	ClCH	Cl	20.7	−62.2	70.4	0.65	2.520
3	$ClCH_2$	Br	3.0	−79.9	61.8	0.52	no TS
4	ClCH	Br	19.1	−72.5	61.0	0.66	2.637
5	$BrCH_2$	Cl	16.6	−67.1	74.6	0.61	2.744
6	BrCH	Cl	33.0	−58.7	72.9	0.73	2.469

[a] Heat of reaction for $Y^- + CH_3X \rightarrow Y + CH_3 + X^-$ from Table 3. [b] Heat of reaction for $Y^- + CH_3X \rightarrow YCH_3 + X^-$ from Table 3. [c] G_{SET} corresponds to the energy difference (B3LYP/6-311+G(2d,p)) between Y^-/CH_3X and the charge transfer state Y/CH_3X^- at the reactant geometry. [d] The parameter $\alpha = 0.5G_{SET}/(G_{SET} - \Delta H_{SET})$. See ref 26. [e] Forming C−C bond distance (Å) in the backside transition state. Reactions **1** and **3** do not have backside transition states.

In Table 7, the reactions are listed in order of increasing rate constants with associated exothermicites as percent of C−X bond cleavage ($\%C-X = 100(d^{\ddagger}_{C-X} - d^{C}_{C-X})/d^{C}_{C-X}$) and $\Delta H^{\ddagger}$.[25] A general trend is found between greater exothermicities from reactants or complexes to products and greater reaction rates. Also, the percent increase in the breaking C−X bond (a small percentage indicates an early transition state) follows the rate constant (the earlier the transition state, the larger the rate constant)

On the other hand, the degree of charge transfer in the backside transition states (Table 5) is a poor indicator of rate constant. The fact that the amount of charge transfer is roughly constant between reactant and backside transition state can be accounted for by the variation in the position of the transition states along the reaction path. A poorer electron donor would have a later transition state which allows more charge to transfer.

The C−X bond in $CHCl^{\bullet -}$ (**2-tsb**) and CH_2Br^- (**5-tsb**) exactly eclipses one of the methyl halide C−H bonds in the backside transition state (Figure 1). In **4-tsb** and **6-tsb**, the eclipsed C_s-symmetry structures are stationary points with two imaginary frequencies. The distortion from C_s symmetry is very slight for **4-tsb,** and the true transition state (C_1 symmetry) is lower in energy by only 0.01 kcal/mol. However, for **6-tsb** the distortion produces a nearly staggered relationship between the C−Br bond and the methyl group (Figure 1) and lowers the energy by 0.05 kcal/mol.

The single-electron-transfer reaction (eq 2) was excluded by Nibbering and co-workers[12] on energetic grounds. Computed thermodynamic values for this pathway (SET) and the subsititution pathway (SUB) are given in Table 8 (ΔH_{SET} and ΔH_{SUB}), where it can be seen that the SET pathways (ΔH_{SET}) for reactions **1-6** are all predicted to be endothermic. An intrinsic reaction coordinate (IRC) from the transition state (**3-tsf**) of reaction **3**, which would give the least endothermic SET products, confirmed that SET products were not formed.

Shaik and co-workers[26] have recently identified a parameter, α, which correlates with the type of reaction, SET or SUB. The parameter α equals $0.5G_{SET}/(G_{SET}-\Delta H_{SET})$, where ΔH_{SET} is the enthalpy of reaction for single

(25) Shaik, S. S.; Schlegel, H. B.; Wolfe, S. *J. Chem. Soc. Chem. Commun.* **1988**, 1322.

(26) (a) Sastry, G. N.; Danovich, D.; Shaik, S. *Angew. Chem., Int. Ed. Engl.* **1996**, *35*, 1098. (b) For a more recent summary, see: Zipse, H. *Angew. Chem. Int. Ed. Engl.* **1997**, *36*, 1697. (c) For more recent work, see: Shaik, S.; Danovich, D.; Sastry, G. N.; Ayala, P. Y.; Schlegel, H. B. *J. Am. Chem. Soc.* **1997**, *119*, 9237.

Table 9. Comparison of Backside and Frontside Activation Enthalpies (kcal/mol)

reactions	backside: $\Delta H^{\ddagger}$ wrt complex[a]	frontside $\Delta H^{\ddagger}$ wrt complex[a]	frontside $\Delta H^{\ddagger}$ wrt reactants[b]
CH_2Cl^-/CH_3Cl (**1**)			16.6
$CHCl^{\bullet -}/CH_3Cl$ (**2**)	0.8	28.0	18.4
CH_2Cl^-/CH_3Br (**3**)			11.8
$CHCl^{\bullet -}/CH_3Br$ (**4**)	-0.7	22.9	12.1
CH_2Br^-/CH_3Cl (**5**)	-0.4	29.4	19.6
$CHBr^{\bullet -}/CH_3Cl$ (**6**)	1.4	32.8	24.3

[a] Activation enthalpies with respect to complex. [b] Activation enthalpies with respect to reactants. Note that reactions **1** and **3** do not form a complex.

electron transfer and G_{SET} corresponds to the vertical energy difference for electron transfer (see Table 8 for details). For values of α greater than about 0.4, the reactions are exclusively substitution.[26] The calculated values of α in Table 8 range from 0.52 in reaction **3** to 0.73 in reaction **6,** which suggests that reactions **1**−**6** will not produce SET products.

Turning attention to frontside attack of the nucleophile on the methyl halide, it should be noted that the activation enthalpies are 29−33 kcal/mol higher than for backside attack (Table 9), which indicates that the reactions are stereospecific. Several other authors have also compared frontside and backside attack for nucleophilic reactions. Glukhovtsev et al.[27] found that backside attack was favored by 39−46 kcal/mol over frontside attack in the identity reactions $X^- + CH_3X$, where X = F, Cl, Br, I. Harder et al.[28] compared inversion and retention transition states for the reactions $X^- + CH_3X$ and $MX + CH_3X$, where M = Li, Na and X = F, Cl. They found that retention (frontside attack) was actually favored over inversion (backside attack) when M = Li and X = F, since this orientation allows the lithium cation to interact simultaneous with both fluorides.

The frontside activation barriers do not decrease in the same order as the backside barriers. Comparing the reaction pairs **1**/**2**, **3**/**4**, and **5**/**6** (Table 9), it can be seen that, with respect to reactants ($CH_2X^-/CHX^{\bullet -}$ and CH_3X), the frontside activation barrier for the second member of each pair ($CHX^{\bullet -}$) is larger. This is perhaps a clearer demonstration that the radical anion is less reactive than the anion. Comparing the reaction pairs **1**/**3** and **2**/**4**, it can be seen that both CH_2Cl^- and $CHCl^{\bullet -}$ have smaller frontside barriers with methyl bromide than methyl chloride, which is in keeping with the relative H_3C-Cl and H_3C-Br bond strengths (see Table 6).

A search was made for frontside reactant complexes. However, it was found that the nucleophiles rotated around the methyl group to form the same complexes as found for backside attack. Another interesting observation is the degree of charge transfer in the frontside transition states. Relative to the backside transition states, much more charge has transferred (Table 5) from the nucleophile (loss of 0.36−0.62 e^-) to the departing halide ion (gain of 0.41−0.58 e^-).

Shaik et al.[29] carried out a computational study which included the backside and frontside transition states for a number of nucleophilic displacement reactions of the type Nu: + $C_2H_6^{\bullet +}$, Nu = H_2O, H_2S, NH_3, PH_3, and HF. They found that the frontside activation barriers were about 20−30 kcal/mol higher than backside barriers.

Table 10. Calculated α-Spin Densities (B3LYP/6-311+G(2d,p)) in Backside (tsb) and Frontside (tsf) Transition States

reaction	α-spin density (e^-)[a] CHX	CHX	CH_3X	CH_3X
$CHCl^{\bullet -} + CH_3Cl$ (**2-tsb**)	0.02	1.08	−0.04	−0.02
$CHCl^{\bullet -} + CH_3Cl$ (**2-tsf**)	0.02	0.46	0.42	0.17
$CHCl^{\bullet -} + CH_3Br$ (**4-tsb**)	0.02	1.06	−0.02	−0.02
$CHCl^{\bullet -} + CH_3Br$ (**4-tsf**)	0.01	0.39	0.50	0.17
$CHBr^{\bullet -} + CH_3Cl$ (**6-tsb**)	0.03	1.07	−0.04	−0.02
$CHBr^{\bullet -} + CH_3Cl$ (**6-tsf**)	0.01	0.55	0.28	0.18

[a] Spin density is given for the underlined atom.

If one compares the forming C−C bond in the backside and frontside transition states for reactions **2**, **4**, **5**, and **6** (Figure 1), it can be seen that the C−C bond in the frontside transitions state is longer than the backside one when the nucleophile is a radical anion (**2**, **4**, **6**), but shorter when the nucleophile is a closed-shell anion (**5**). Since the frontside activation barriers are much higher than the backside ones, it would seem reasonable that the attacking nucleophile would have to approach the methyl group more closely from the front to affect the halide displacement. Why then are the C−C bonds in reactions **2**, **4**, and **6** longer for the frontside attack?

Another difference between backside and frontside transition states can be seen from the orientation of the attacking nucleophile. In **5-tsf**, the CH_2Br^- group leads with the lone pair directed toward the methyl group. In contrast, the $CHX^{\bullet -}$ fragments in **2-tsf**, **4-tsf**, and **6-tsf** all lead with the unpaired electron toward the methyl group. The difference between backside and frontside attack can be clearly seen in the spin densities of the corresponding transition states (Table 10). In backside attack (**2-tsb**, **4-tsb**, **6-tsb**), the unpaired spin density remains almost completely on the carbon atom of the nucleophile. In frontside attack (**2-tsf**, **4-tsf**, **6-tsf**), the unpaired spin density is distributed between the two carbons. The distinction between the two mechanisms for reaction of a radical anion is that backside attack leads to formation of a two-center, two-electron (2c−2e) C−C bond while frontside attack leads to the initial formation of a two-center, one-electron (2c−1e) C−C bond. The origin of the difference is due to the different steric requirements in the two approaches. The much greater steric demands in frontside attack favors the formation the 2c−1e C−C bond, which has a much longer intrinsic length[30] than a 2c−2e bond. As the reaction proceeds toward products, the lone pair on the CHX fragment and the 2c−1e orbital will interact to form a 2c−2e C−C bond and a radical center on carbon.

Conclusions

Density function theory has been used to probe the reactivity difference between radical anion ($CHCl^{\bullet -}$ and $CHBr^{\bullet -}$) and anions (CH_2Cl^- and CH_2Br^-) in the S_N2 reaction with methyl halides (CH_3Cl and CH_3Br). In agreement with experiment, the calculations predict that the CH_2X^- anions are more reactive than the $CHX^{\bullet -}$

(27) Glukhovtsev, M. N.; Pross, A.; Schlegel, H. B.; Bach, R. D.; Radom, L. *J. Am. Chem. Soc.* **1996**, *118*, 11258.

(28) Harder, S.; Streitwieser, A.; Petty, J. T.; Schleyer, P. v. R. *J. Am. Chem. Soc.* **1995**, *117*, 3253.

(29) Shaik, S.; Reddy, A. C.; Ioffe, A.; Dinnocenzo, J. P.; Danovich, D.; Cho, J. K. *J. Am. Chem. Soc.* **1995**, *117*, 3205.

(30) The C−C bond in $C_2H_6^{\bullet +}$ at the UMP2/6-31G* level is 1.921 Å. See ref 29.

radical anions. Relative rate constants, computed with free energies of activation, are in good agreement with experimental results. The best indicator of reactivity is the degree of charge transfer in the ion−molecule complex. This indicator is a function of the donating ability of the nucleophile and the accepting ability of the electrophile. Ionization energies (IE), proton affinities (PA), bond dissociation enthalpies (BDE), and methyl cation affinities of fragments have also been calculated.

From a comparison of the backside and frontside transition states, the reactions are predicted to proceed stereospecifically with inversion of configuration. The radical anions are predicted to react with the methyl halide with a different mechanism in backside and frontside attack. In backside attack (where steric demands are low), the radical anion leads with its lone pair to form a two-center, two-electron C−C bond. In frontside attack (where steric demands are high), the radical anion leads with an unpaired electron to form an initial two-center, one-electron C−C bond.

Acknowledgment. Computer time for this study was made available by the Alabama Supercomputer Network. I thank Drs. Tom Webb and Metin Balci for carefully reading the manuscript. Dr. Nico J. R. van Eikema Hommes is thanked for making Molecule available, which was used for drawing the structures in Figure 1.

Supporting Information Available: Optimized Cartesian coordinates (B3LYP/6-31+G(d)) for species in Table 2 (Table S1) and total energies (Table S2) and relative energies (Table S3) of species optimized at the MP2/6-31+G(d) level are available (7 pages). This material is contained in libraries on microfiche, immediately follows this article in the microfilm version of the journal, and can be ordered from the ACS; see any current masthead page for ordering instructions.

JO970163E